

COMMUNICATION

A zinc-based oxysulfide photocatalyst $\text{SrZn}_2\text{S}_2\text{O}$ capable of reducing and oxidizing water †

Received 00th January 20xx,
Accepted 00th January 20xx

DOI: 10.1039/x0xx00000x

Shunta Nishioka,^{a,b} Tomoki Kanazawa,^{a,b} Kengo Shibata,^a Yoshihiro Tsujimoto,^{*c} Hans-Conrad zur Loye^d and Kazuhiko Maeda^{*a}

Although Zn-based binary semiconductors such as ZnO and ZnS are photocatalytically unstable toward water oxidation, we found that mixed-anionization successfully addressed this issue. This report shows that an oxysulfide $\text{SrZn}_2\text{S}_2\text{O}$ functions as a photocatalyst to reduce and oxidize water under band-gap irradiation without noticeable decomposition of the material.

Many semiconductor photocatalysts have been investigated for converting solar energy into H_2 through water splitting.^{1–3} Semiconductors that consist of early transition metal cations with d^0 electronic configurations (e.g., Ti^{4+} , Nb^{5+} , or Ta^{5+}) or typical d^{10} metal cations (e.g., Ga^{3+} , Sn^{4+} , or Sb^{5+}) as principal components have been reported as photocatalysts that can reduce and oxidize water.^{1–12}

Zn^{2+} -based semiconductors are expected to be active as photocatalysts for water reduction and oxidation, but there is no report on such photocatalysts with reasonable activity for water oxidation. For example, it has been reported that ZnO and ZnS showed high photocatalytic activity for H_2 evolution, while O_2 evolution could not be driven due to photocorrosion of the material caused by photogenerated holes.^{13–15} In the cases of ZnO -based materials, the self-decomposition could be suppressed by forming solid-solution with GaN ,¹⁶ making a superlattice structure with In_2O_3 ,¹⁷ or doping of foreign ions.¹⁸

Mixed-anionization sometimes leads to unexpected results,¹⁹ as exemplified by the GaN-ZnO solid solution; both GaN and ZnO are wide-gap semiconductors, but the solid solution of them results in a visible-light-absorbing new

material.¹⁶ An oxyfluoride (oxide-fluoride) that has an unprecedentedly small band gap has been reported as well.¹⁰

In this work, we report that for the Zn-based oxysulfide, $\text{SrZn}_2\text{S}_2\text{O}$, such a mixed-anionization strategy leads to the discovery of a Zn-based oxysulfide photocatalyst $\text{SrZn}_2\text{S}_2\text{O}$ that possesses not only high photocorrosive resistance but also the capability to reduce and oxidize water under band-gap irradiation. The Zn-based oxysulfide $\text{SrZn}_2\text{S}_2\text{O}$ has recently been reported to crystallize in the polar space group $Pmn2_1$ that consists of corner-shared ZnS_3O tetrahedra, as shown in Fig. 1A.²⁰ The lower part of the conduction band of $\text{SrZn}_2\text{S}_2\text{O}$ is derived from Zn-4s , Zn-4p , and Sr-4d hybridized orbitals, whereas the upper part of the valence band is mainly composed of hybridized orbitals of O-2p and S-3p (Fig. 1B). The direct band gap (ca. 3.9 eV) corresponds to electron transitions from S-3p to Zn-4s orbitals.

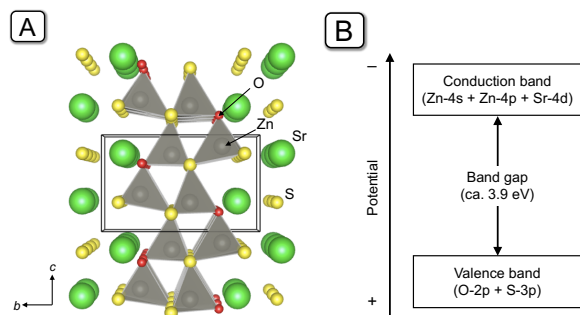


Fig. 1. (A) Crystal structure and (B) schematic illustration of band structure of $\text{SrZn}_2\text{S}_2\text{O}$.

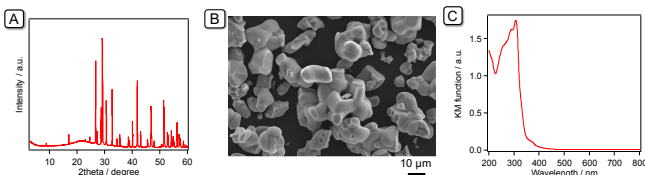


Fig. 2. (A) XRD patterns, (B) SEM images and (C) DR spectrum of as-prepared $\text{SrZn}_2\text{S}_2\text{O}$.

^a Department of Chemistry, School of Science, Tokyo Institute of Technology, 2-12-1 NE-2 Ookaya-ma, Meguro-ku, Tokyo 152-8550, Japan

^b Japan Society for the Promotion of Science, Kojimachi Business Center Building, 5-3-1 Kojimachi, Chiyoda-ku, Tokyo 102-0083, Japan

^c Research Center for Functional Materials, National Institute for Materials Science (NIMS), 1-1 Namiki, Tsukuba, Ibaraki 305-0044, Japan

^d Department of Chemistry and Biochemistry, University of South Carolina, Columbia, South Carolina 29208, United States

† Electronic Supplementary Information (ESI) available. See DOI: 10.1039/x0xx00000x

Polycrystalline $\text{SrZn}_2\text{S}_2\text{O}$ was synthesized through a solid-state reaction using SrO , Zn , and S as precursors, according to the previously reported method.²⁰ X-ray diffraction (XRD) analysis indicated that $\text{SrZn}_2\text{S}_2\text{O}$ was obtained as a single phase product (Fig. 2A). A scanning electron microscopy (SEM) image of the material is shown in Fig. 2B, unveiling that the particle size of $\text{SrZn}_2\text{S}_2\text{O}$ ranged from several micrometer to several tens of micrometer. The Brunauer–Emmett–Teller (BET) surface area of the synthesized $\text{SrZn}_2\text{S}_2\text{O}$ was $0.3 \text{ m}^2 \text{ g}^{-1}$. The UV-visible diffuse reflectance (DR) spectrum of $\text{SrZn}_2\text{S}_2\text{O}$ is shown in Fig. 2C. The absorption edge is at approximately 320 nm and a shoulder is observed at 400 nm, which was attributed to an impurity state, as discussed in the previous report.²⁰

The flat-band potential of $\text{SrZn}_2\text{S}_2\text{O}$ was measured by means of electrochemical impedance spectroscopy. As shown in Fig. 3A, a positive slope of Mott–Schottky plot indicates n-type semiconducting character for $\text{SrZn}_2\text{S}_2\text{O}$. The flat-band potentials measured at different pH conditions increased with an increase in the pH of the electrolyte solution (Fig. 3A inset). The flat-band potential of $\text{SrZn}_2\text{S}_2\text{O}$ was thus estimated to be -0.3 V (vs. Ag/AgCl at pH 0), which corresponds to -0.1 V vs. NHE. The energy level of the conduction band minimum (CBM) of $\text{SrZn}_2\text{S}_2\text{O}$ was determined to be approximately $-0.3 \pm 0.1 \text{ V}$ vs. NHE at pH 0, considering a potential difference of $0.1\text{--}0.3 \text{ V}$ between flat-band potential and the CBM in an n-type semiconductor.²² The energy level of the valence band maximum (VBM) was calculated to be $3.6 \pm 0.1 \text{ V}$, taking into consideration that the VBM and CBM energy levels should be separated by 3.9 V . A schematic illustration of the band-gap structure of $\text{SrZn}_2\text{S}_2\text{O}$ is depicted in Fig. 3B. The potentials of CBM and VBM straddle the proton reduction and water oxidation potentials (H^+/H_2 , 0 V ; $\text{O}_2/\text{H}_2\text{O}$, $+1.23 \text{ V}$ vs. NHE pH 0).

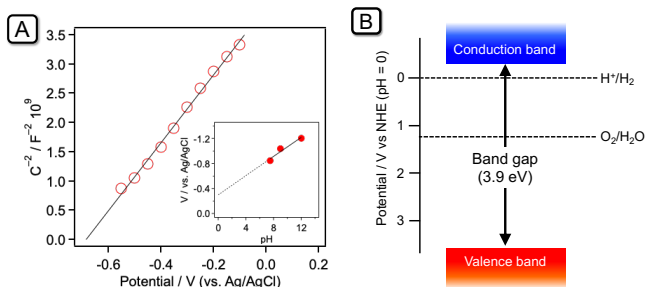


Fig. 3. (A) Mott–Schottky plot of $\text{SrZn}_2\text{S}_2\text{O}$ recorded at 1 kHz in aqueous Na_2SO_4 solution (0.1 M) with different pH. (B) Schematic band structure diagram of $\text{SrZn}_2\text{S}_2\text{O}$, along with some redox potentials.

Using the as-prepared $\text{SrZn}_2\text{S}_2\text{O}$ powders, photocatalytic reactions were performed. Fig. 4A shows irradiation wavelength dependence of photocatalytic H_2 evolution from aqueous Na_2S (10 mM) and Na_2SO_3 (10 mM) mixed solution with Pt cocatalyst modification (0.1 wt%). H_2 evolution was observed only under UV light irradiation ($\lambda > 200 \text{ nm}$ or 300 nm), and the H_2 evolution rate was decreased with increasing the irradiation wavelength. Under irradiation with wavelength longer than 400 nm , $\text{SrZn}_2\text{S}_2\text{O}$ hardly evolved any H_2 . This change in the H_2 evolution rate corresponds to the optical property of the material (Fig. 2C), meaning that the reaction was driven by light absorption of

$\text{SrZn}_2\text{S}_2\text{O}$. The reaction stability was also measured by changing the reactant solution to a fresh one after each reaction (Fig. 4B). Interestingly, the H_2 evolution was enhanced by repeated use and that the H_2 evolution rate recorded in the 3rd run was twice that of the 1st run.

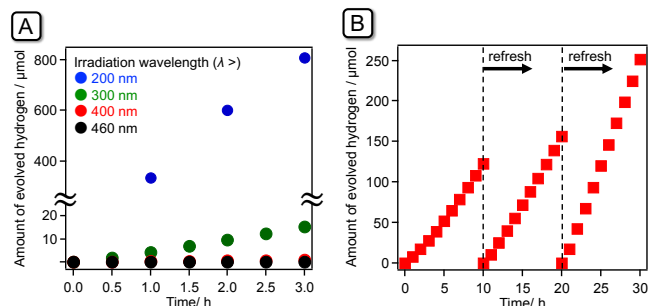


Fig. 4. Time course of H_2 evolution using $\text{Pt}/\text{SrZn}_2\text{S}_2\text{O}$ in aqueous Na_2S and Na_2SO_3 mixed solution. (A) Irradiation wavelength dependence, and (B) time course of the consecutive reactions under UV light ($\lambda > 300 \text{ nm}$). Reaction conditions: catalyst, 50 mg (0.1 wt% Pt photodeposition); reactant solution, aqueous Na_2S (10 mM) and Na_2SO_3 (10 mM), 140 mL; light source, Xe lamp (300 W).

To investigate the chemical stability after the repeated reactions, XRD and DRS measurements were conducted. The diffraction peak positions of the reacted photocatalyst remained almost unchanged (Fig. S1A). However, the peak intensities had slightly changed. This result indicates that the crystal orientation changed during the reaction, while maintaining the original crystal structure of $\text{SrZn}_2\text{S}_2\text{O}$. UV-vis DRS recorded after the reaction was consistent with that recorded before the reaction, although a small increase in the background level is observed at longer wavelengths, which was due to the deposited Pt (Fig. S1B).

To understand the increased activity observed during the reaction without a noticeable change in the crystal structure and optical absorption behavior, we investigated the physicochemical properties of $\text{SrZn}_2\text{S}_2\text{O}$ after washing the sample with water for at least 1 week at room temperature. XRD and DRS were essentially the same as those of the after-reaction specimens (Fig S1), however the absorption due to the impurity state (observed at 320–400 nm) virtually disappeared in the water-washed sample. In the after-reaction specimen, the reduction of the impurity absorption was not very clear, most likely because of the presence of Pt on $\text{SrZn}_2\text{S}_2\text{O}$. However, the morphology of the water-washed specimen dramatically changed, as shown in Fig. 4. It is clear that most of the particles of $\text{SrZn}_2\text{S}_2\text{O}$ became smaller, their size was reduced to only several micrometers, accompanied by the emergence of a surface step structure. The particle size reduction was also confirmed by BET measurement, which indicated that the water-washed sample had a surface area of $3 \text{ m}^2 \text{ g}^{-1}$, 10 times larger than the as-prepared powder.

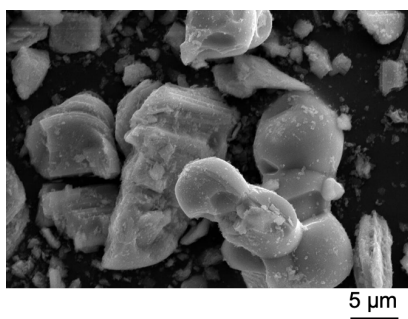


Fig. 4. SEM images of $\text{SrZn}_2\text{S}_2\text{O}$ after the photocatalytic H_2 evolution reaction.

On the basis of these results, we concluded that the enhancement of the photocatalytic H_2 evolution activity during the repeated reaction arose from the reduction of the particle size of $\text{SrZn}_2\text{S}_2\text{O}$ that created a larger specific surface area. A larger specific surface area, in principle, reflects a greater number of reaction sites, which leads to a higher photocatalytic activity.² The discussion in the following sections applies to the water-washed $\text{SrZn}_2\text{S}_2\text{O}$ samples.

Table 1 lists the rates of photocatalytic H_2 and O_2 evolution using water-washed $\text{SrZn}_2\text{S}_2\text{O}$ from aqueous Na_2S – Na_2SO_3 or AgNO_3 solution under UV light irradiation, along with ZnS and ZnO for comparison. All these samples evolved H_2 from aqueous solution with the aid of a Pt cocatalyst. Apparent quantum yield of $\text{SrZn}_2\text{S}_2\text{O}$ for H_2 evolution was 11% under 300 nm irradiation.

On the other hand, O_2 evolution was observed only for $\text{SrZn}_2\text{S}_2\text{O}$ and not for the simple mixture of ZnS and ZnO , even after the addition of IrO_2 , which is one of the best-performing cocatalysts for water oxidation.²³ ZnO is known to undergo decomposition during water oxidation reaction.¹⁵ After the water oxidation reaction in an AgNO_3 aqueous solution, the diffraction patterns of ZnO almost disappeared, accompanied by the generation of Ag metal peaks (Fig. S2). This indicates that ZnO decomposed and that Ag metal was generated during the reaction. Zn ions probably existed as $\text{Zn}(\text{NO}_3)_2$ in the reactant solution.

Table 1. Photocatalytic H_2 and O_2 evolution using $\text{SrZn}_2\text{S}_2\text{O}$, ZnS and ZnO under UV light.^a

Photocatalyst	Amount of gas evolved after 3 h / μmol	
	H_2^c	O_2^d
$\text{SrZn}_2\text{S}_2\text{O}$	67.8	26.9 ^e
ZnS	34.3	< 1
ZnO^b	2.1	– ^f

^a Reaction conditions: catalyst, 50 mg; light source, Xe lamp (300 W, $\lambda > 300$ nm). ^b Commercial ZnO (Kojundo Chemical Laboratory, > 99.99%) was used. ^c Cocatalyst loading, Pt 0.1 wt% in-situ photodeposition; reactant solution, aqueous Na_2S (10 mM) and Na_2SO_3 (10 mM), 140 mL. ^d Cocatalyst loading, IrO_2 1.0 wt% impregnation; reactant solution, aqueous AgNO_3 (10 mM), 140 mL. ^e Catalyst was used 30 mg. ^f Decomposed (see Fig. S3).

The water oxidation reaction by $\text{SrZn}_2\text{S}_2\text{O}$ was further examined with and without IrO_2 cocatalyst loading. The oxidation state of the loaded Ir species was close to that of the IrO_2 reference, as revealed by X-ray photoelectron spectroscopy measurement (XPS, Fig. S3A). Transmission electron microscopy (TEM) showed that the particle size of the loaded IrO_2 was less

than 5 nm (Fig. S3B). Fig. 5A shows the time course of O_2 evolution using $\text{SrZn}_2\text{S}_2\text{O}$ powder from aqueous AgNO_3 solution under UV irradiation. O_2 evolution reaction was enhanced dramatically by IrO_2 cocatalyst loading. The XRD patterns of $\text{SrZn}_2\text{S}_2\text{O}$ after the reaction are shown in Fig. 5B. Both after-reaction specimens showed clear diffraction patterns of $\text{SrZn}_2\text{S}_2\text{O}$, with diffraction peaks attributed to Ag metal and a very small Ag_2S peak (enlarged in Fig. 5C). Metallic Ag was generated by the photoreduction of Ag^+ ions (and concomitant water oxidation), while Ag_2S might be formed by a reaction with dissolved S^{2-} ions from the $\text{SrZn}_2\text{S}_2\text{O}$ surface. It is clear that the IrO_2 modification intensified the Ag metal peak, but reduced the Ag_2S peak (Fig. 5C), indicating that the IrO_2 modification enhances the Ag^+ reduction (i.e., water oxidation to form O_2) while suppressing S^{2-} dissolution.

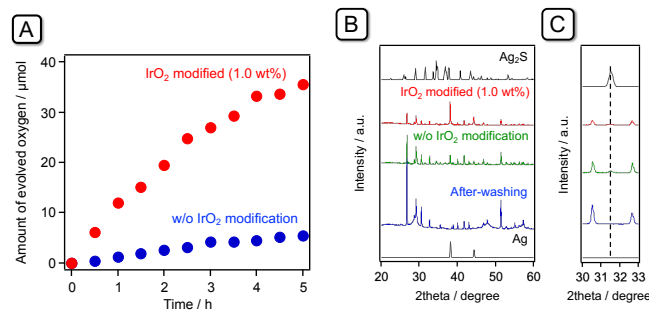


Fig. 5. (A) Time course of O_2 evolution using $\text{SrZn}_2\text{S}_2\text{O}$ in aqueous AgNO_3 solution under UV light w/ or w/o IrO_2 modification. (B) XRD patterns of $\text{SrZn}_2\text{S}_2\text{O}$ after-washing, after reaction w/ and w/o IrO_2 modification. (C) is an enlarged view of (B). Reaction conditions in (A): catalyst, 30 mg (w/ or w/o 1.0 wt% IrO_2 impregnation); reactant solution, aqueous AgNO_3 (10 mM), 140 mL; light source, Xe lamp (300 W, $\lambda > 300$ nm). ICSD numbers in (B): Ag, 18173; Ag_2S , 182916.

These results strongly suggest that O_2 evolution during the reaction arose not from photocorrosion of $\text{SrZn}_2\text{S}_2\text{O}$ but rather almost exclusively from the photocatalytic oxidation of water. An additional investigation on the origin of the generated O_2 focused on the O_2 evolution reaction from ^{18}O -enriched H_2O . Fig. S4 shows the GC-MS plot of gas phase O_2 generated during the oxidation of H_2^{18}O by IrO_2 -modified $\text{SrZn}_2\text{S}_2\text{O}$. A signal of $^{18}\text{O}_2$ ($m/z = 36$) was clearly observed. As listed in Table S1, the signal intensity of $^{18}\text{O}_2$ was much larger in the case of H_2^{18}O than that for the reaction using unlabeled water. This result clearly demonstrates that water was actually photooxidized by the IrO_2 / $\text{SrZn}_2\text{S}_2\text{O}$ to yield O_2 molecules.

In summary, we found a new Zn-based oxysulfide photocatalyst, $\text{SrZn}_2\text{S}_2\text{O}$, which individually produced both H_2 and O_2 from water with the aid of a proper cocatalyst. This is the first example of a Zn-based oxysulfide material that is photocatalytically active for both H_2 and O_2 evolution in aqueous solutions.

This work was supported by a Grant-in-Aid for Scientific Research on Innovative Area "Mixed Anion (Project JP16H06440, JP16H06441, JP17H05493 and JP19H04711)" (JSPS). It was also partially supported by a Grant-in-Aids for Scientific Research (B) (Project JP19H02511), and for Challenging Research (Exploratory) (JP17K19169). S.N. and T.K. wish to acknowledge support by a JSPS Fellowship for Young

Scientists (Project JP18J10457 and JP18J10548). The authors thank the Suzukakedai Materials Analysis Division, Technical Department, Tokyo Institute of Technology for assistance in GC-MS experiments. H.-C.z.L. acknowledges support from the National Science Foundation under award DMR-1806279

21 **30**, 6486–6493.
B. Liang, N. Zhang, C. Chen, X. Liu, R. Ma, S. Tong, Z. Mei, V. A. L. Roy, H. Wang and Y. Tang, *Catal. Sci. Technol.*, 2017, **7**, 1000–1005.

22 Y. Matsumoto, *J. Solid State Chem.*, 1996, **126**, 227–234.

23 A. Harriman, I. J. Pickering, J. M. Thomas and P. A. Christensen, 1988, **84**, 2795–2806.

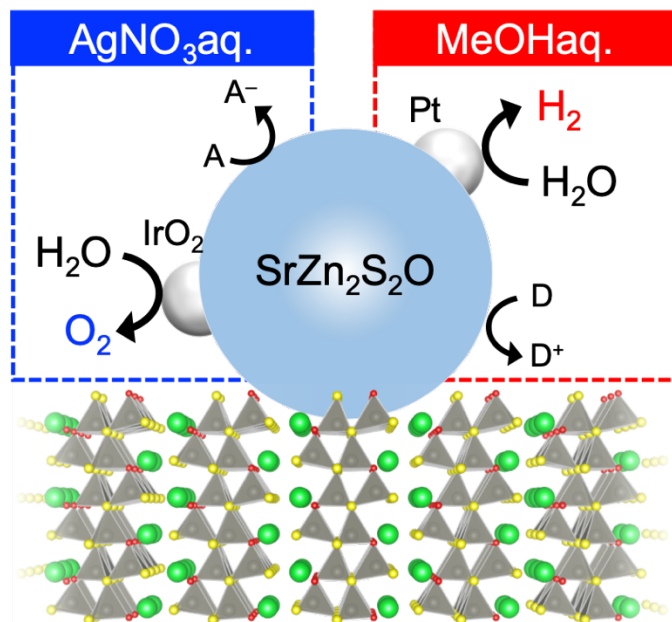
Conflicts of interest

There are no conflicts to declare.

Notes and references

- 1 A. Kudo and Y. Miseki, *Chem. Soc. Rev.*, 2009, **38**, 253–278.
- 2 K. Maeda, *J. Photochem. Photobiol. C*, 2011, **12**, 237–268.
- 3 T. Hisatomi, J. Kubota and K. Domen, *Chem. Soc. Rev.*, 2014, **43**, 7520–7535.
- 4 K. Ogisu, A. Ishikawa, Y. Shimodaira, T. Takata, H. Kobayashi and K. Domen, *J. Phys. Chem. C*, 2008, **112**, 11978–11984.
- 5 T. Suzuki, T. Hisatomi, K. Teramura, Y. Shimodaira, H. Kobayashi and K. Domen, *Phys. Chem. Chem. Phys.*, 2012, **14**, 15475–15481.
- 6 K. Maeda and K. Domen, *J. Phys. Chem. C*, 2007, **111**, 7851–7861.
- 7 K. Shimizu, H. Kato, M. Kobayashi and M. Kakihana, *Appl. Catal. B*, 2017, **206**, 444–448.
- 8 A. P. Black, H. Suzuki, M. Higashi, C. Frontera, C. Ritter, C. De, A. Sundaresan, R. Abe and A. Fuentes, *Chem. Commun.*, 2018, **54**, 1525–1528.
- 9 C. Pan, T. Takata, M. Nakabayashi, T. Matsumoto, N. Shibata, Y. Ikuhara and K. Domen, *Angew. Chem. Int. Ed.*, 2015, **54**, 2955–2959.
- 10 R. Kuriki, T. Ichibha, K. Hongo, D. Lu, R. Maezono, H. Kageyama, O. Ishitani, K. Oka and K. Maeda, *J. Am. Chem. Soc.*, 2018, **140**, 6648–6655.
- 11 A. Ishikawa, T. Takata, T. Matsumura, J. N. Kondo, M. Hara, H. Kobayashi and K. Domen, *J. Phys. Chem. B*, 2004, **108**, 2637–2642.
- 12 K. Ogisu, A. Ishikawa, K. Teramura, K. Toda, M. Hara and K. Domen, *Chem. Lett.*, 2007, **36**, 854–855.
- 13 A. J. Bard and M. S. Wrighton, *J. Electrochem. Soc.*, 1977, **124**, 1706–1710.
- 14 D. J. Fermín, E. A. Ponomarev and L. M. Peter, *J. Electroanal. Chem.*, 1999, **473**, 192–203.
- 15 J. Doménech and A. Prieto, *J. Phys. Chem.*, 1986, **90**, 1123–1126.
- 16 K. Maeda, T. Takata, M. Hara, N. Saito, Y. Inoue, H. Kobayashi and K. Domen, *J. Am. Chem. Soc.*, 2005, **127**, 8286–8287.
- 17 A. Kudo and I. Mikami, *Chem. Lett.*, 1998, **27**, 1027–1028.
- 18 C. B. Ong, L. Y. Ng and A. W. Mohammad, *Renewable Sustainable Energy Rev.*, 2018, **81**, 536–551.
- 19 H. Kageyama, K. Hayashi, K. Maeda, J. P. Attfield, Z. Hiroi, J. M. Rondinelli and K. R. Poeppelmeier, *Nature Commun.*, 2018, **9**, 772.
- 20 Y. Tsujimoto, C. A. Juillerat, W. Zhang, K. Fujii, M. Yashima, P. S. Halasyamani and H. C. zur Loye, *Chem. Mater.*, 2018,

TOC



Even though Zn-based binary semiconductors, such as ZnO and ZnS, are unstable for water oxidation, the oxysulfide $SrZn_2S_2O$ is an active photocatalyst for both water oxidation and water reduction.